Inorganic Chemistry

Article

pubs.acs.org/IC

Novel Blue-Emitting $Na_xCa_{1-x}Al_{2-x}Si_{2+x}O_8:Eu^{2+}$ (x = 0.34) Phosphor with High Luminescent Efficiency for UV-Pumped Light-Emitting Diodes

Ga-yeon Lee,[†] Ji Yeon Han,[†] Won Bin Im,[‡] Sang Hoon Cheong,[†] and Duk Young Jeon*[,†]

[†]Department of Materials Science and Engineering, Korea Advanced Institute of Science and Technology, Daejeon 305-701, Republic of Korea

[‡]School of Materials Science and Engineering, Chonnam National University, 300 Yongbong-Dong, Buk-Gu, Gwangju, 500-757, Republic of Korea

Supporting Information

ABSTRACT: A novel blue-emitting phosphor, $Na_{0.34}Ca_{0.66}Al_{1.66}Si_{2.34}O_8:Eu^{2+}$ (NCASO:Eu^{2+}), was prepared by a wet chemical synthesis method based on the hydrolysis of tetraorthosiliate (TEOS) and confirmed the formation of NCASO:Eu^{2+} from Rietveld analysis. Photoluminescence (PL) results showed that the phosphor can be efficiently excited by UV light from 250 to 420 nm, and emitted bright broad blue emission, which has maximum intensity at around 445 nm. Under 365 nm excitation, the PL emission intensity area of optimized NCASO:Eu^{2+} was found to be 99.72% of that of a commercial $BaMgAl_{10}O_{17}:Eu^{2+}$ (BAM:Eu^{2+}) phosphor. Moreover, the optical absorbance, internal quantum efficiency, and external quantum efficiency of NCASO:Eu^{2+} were calculated to be 112%, 94%, and 105% of that of the commercial BAM:Eu^{2+} phosphor, respectively. The WLEDs were fabricated using the blue NCASO:Eu^{2+} phosphor, a green-emitting β−SiAlON:Eu^{2+}, and a red-emitting $CaAlSiN_3:Eu^{2+}$ phosphors with a near-UV chip. The WLED device exhibited an excellent color−rendering index R_a of 94 at a correlated color temperature of 5956 K with CIE coordinates of x = 0.323, y = 0.335. These results suggest that NCASO:Eu^{2+} is a promising blue-emitting phosphor for UV LED applications.

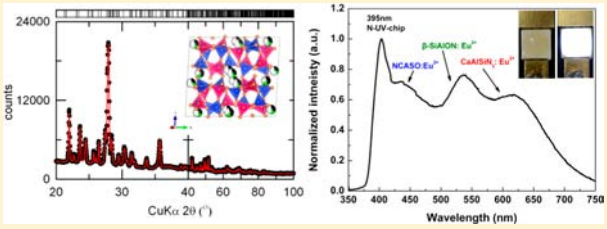

1. INTRODUCTION

Light-emitting diode (LED) with phosphors to generate white light is an important technology in the lighting industry because of LEDs having advantages such as energy saving, reliability, maintenance, and safety.[1,2] Typically, the commercial white light-emitting diodes (WLEDs) use a combination of a blue emitting InGaN chip and a yellow emitting $Y_3Al_5O_{12}:Ce^{3+}$ (YAG:Ce^{3+}) phosphor. However, this method has some disadvantages such as a high correlated color temperature (CCT ∼7750 K) and a low color-rendering index (CRI ∼70−80) due to the lack of red emission in the visible region.[3,4] To improve the CRI and tune the CCT value, near-UV LEDs, or UV LEDs coated with red-, green-, and blue-emitting phosphors have attracted much attention. As a result, recent research has focused on finding phosphors, which can be excited by UV sources. In addition, the performances of WLEDs strongly depend on the luminescence properties of phosphors used. In other words, phosphors play a key role in producing high-quality white lighting. Therefore, as conversion luminescent materials in WLEDs, phosphor needs to have high conversion efficiency, appropriate emission colors, and high chemical stability.[4−7]

For these reasons, recently aluminosillcate-based phosphors have drawn much attention for their excellent luminescence properties such as stable crystal structure and high chemical and physical stability.[8,9] Examples of these known aluminosilicate phosphors are $CaAl_2Si_2O_8:Eu^{2+}$, Mn^{2+},[10] $NaAlSiO_4:Eu^{2+}$,[11] $CaAl_2Si_2O_8:Eu^{2+}$,[12] $CaAl_2SiO_6:Ce^{3+}$, Tb^{3+},[9] $BaMgAl_6Si_9O_{30}:Eu^{2+}$, Tb^{3+}, Mn^{2+} and $Na_{2-x}Al_{2-x}Si_xO_4:Eu^{2+}$.[13,14] In this article, a new phosphor $Na_xCa_{1-x}Al_{2-x}Si_{2+x}O_8:Eu^{2+}$ (x = 0.34) (NCASO:Eu^{2+}), which is potentially applicable to white LEDs, is reported. To the best of our knowledge, there has been no reported study on NCASO:Eu^{2+}, which is included in the plagioclase feldspar crystal structure, as a phosphor host in the literature. The plagioclase feldspars group is also based on the aluminosilicate composition and shows the excellent thermal stability.[15−20] On the basis of the above consideration, NCASO has the sufficient possibility to become an efficient luminescent host material.

The structure of NCASO:Eu^{2+} phosphor consists of a 3D framework of corner-shared tetrahedral and each tetrahedron is centered by Si^{4+} or an Al^{3+} ions. The oxygen ions are located at each corner of tetrahedral and join two tetrahedrals. Moreover, the Si^{4+} ions are frequently replaced by Al^{3+} ions, and the charge balance is maintained by alkali-metal or alkaline-earth

Received: May 9, 2012
Published: September 24, 2012

ions that occupy the crystal site formed by silica/alumina tetrahedra.[15,16] In this crystal structure, Eu^{2+} ions are expected to take the Na^+/Ca^{2+} sites in considering their ionic radii. In this article, we prepared NCASO:Eu^{2+} phosphor via sol–gel methods. Also, the luminescence properties were reported that effect of Eu^{2+} concentration and its thermal stability were investigated. In addition, white-light LED possessing excellent CRI values and warm correlated color temperatures were fabricated using phosphor blends of green-emitting β–SiAlON:Eu^{2+} phosphor and red-emitting $CaAlSiN_3$:Eu^{2+} phosphor on n-UV LED.

2. EXPERIMENTAL SECTION

2.1. Synthesis. NCASO:Eu^{2+} phosphor was synthesized by a wet chemical synthesis method based on the hydrolysis of tetraethyl orthosilicate (TEOS), which is generally used as a Si source according to the following reaction equation; $Si(OC_2H_5)_4 + 4H_2O \rightarrow Si(OH)_4 + 4C_2H_5OH$ in ethanol.[14]

The starting materials used for preparation of the phosphor were sodium nitrate ($NaNO_3 \geq 99.99\%$, Aldrich), europium-(III) chloride hexahydrate ($EuCl_2{\cdot}6H_2O \geq 99.99\%$, Aldrich), calcium nitrate ($Ca(NO_3)_2{\cdot}9H_2O \geq 99.99\%$, Aldrich), aluminum nitrate nonahydrate ($Al(NO_3)_3{\cdot}9H_2O \geq 98\%$, Aldrich), tetraethyl orthosilicate (TEOS, 99.999%, Aldrich). First, all materials were dissolved in deionized water except for TEOS. Second, TEOS dissolved in ethanol was added to the above solution and they were thoroughly mixed together. The mixture was dehydrated in an oven at 120 °C for about 24 h until the solvent dried completely. The dried powders were fired at 1400 °C in a reducing atmosphere of a mixture of H_2 (5%) and N_2 (95%) for 3 h.

2.2. Characterizations. To investigate its luminescent properties, photoluminescence (PL) and photoluminescence excitation (PLE) were performed by using an F-7000 Hitachi fluorescence spectophotometer PL system equipped with a xenon lamp (500 W) as an excitation source. The X-ray diffraction (XRD) data was obtained over a range of $20° \leq 2\theta \leq 100°$ at step of 0.026° with Cu-Kα radiation (Philips X'Pert). Crystal structure refinement employed the Rietveld method as implemented in the General Structure Analysis System (GSAS) software suite. For time-resolved PL measurements, Fluorescence Lifetime Spectrometer (TCSPC) [Edinburgh Instruments, Wales] was used.

2.3. LED Chip Fabrication. LED was fabricated by using near-UV LED chip (λ_{max} = 395 nm) with NCASO:Eu^{2+} phosphor, green-emitting β–SiAlON:Eu^{2+}, and red-emitting $CaAlSiN_3$:Eu^{2+} phosphors. Optical properties such as luminescence spectra, color-rendering index (R_a), and Commission International de l'Eclairage (CIE) color coordinates for samples were recorded by a DARSA PRO 5100 PL system (PSI Scientific Co. Ltd., Korea) with Xe lamp (500 W).

3. RESULTS AND DISCUSSION

3.1. Structural Properties of NCASO:Eu^{2+} Phosphor. Figure 1 shows the TGA/DSC curve of NCASO:Eu^{2+} powder with stoichiometric proportions from room temperature up to 1400 °C with a heating rate of 10 °C min^{-1} in nitrogen atmosphere. The weight loss was mainly caused by the release of H_2O and NO_3 from the decomposition of the starting material before 600 °C. From the DSC pattern (red line) in Figure 1, the DSC shows an obvious exothermic peak at around 1100 °C, which may be connected to the crystallization of

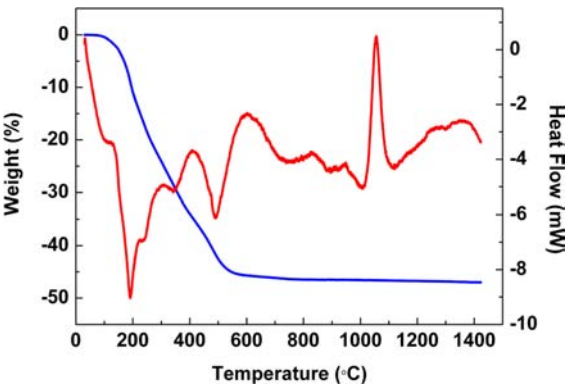

Figure 1. TGA and DSC curves of NCASO:Eu^{2+} from room temperature up to 1400 °C with a heating rate of 10 °C min^{-1} in nitrogen gas.

NCASO:Eu^{2+}. Moreover, the next exothermic peak at around 1300 °C may be due to the phase formation of NCASO:Eu^{2+}. Thus, we decided the sintering temperature of NCASO:Eu^{2+} samples over 1300 °C.[15] In addition, XRD patterns and PL spectra data of NCASO:Eu^{2+} phosphor at different temperature are given in Figure S1 of the Supporting Information. From the result, the synthesis temperature was selected to 1400 °C.

Figure 2 represents a unit cell of NCASO phosphor. Green, black, blue, red, and orange spheres indicate Na, Ca, Si, Al, and

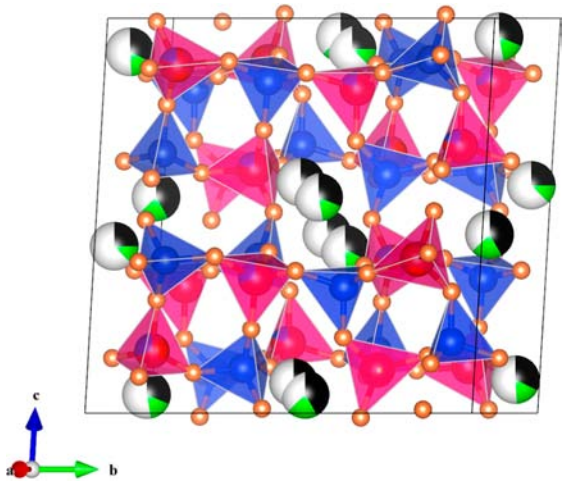

Figure 2. Unit-cell representation of $Na_{0.34}Ca_{0.66}Al_{1.66}Si_{2.34}O_8$. Green, black, blue, red, and orange spheres represent Na, Ca, Si, Al, and O atoms, respectively. Blue and red polyhedrals are displayed by Si and Al tetrahedral.

O atoms, respectively. NCASO:Eu^{2+} phosphors follow the plagioclase feldspar crystal structure, which is constructed of a 3D framework of corner-shared SiO_4 tetrahedral with each Si^{4+} ion being surrounded by four oxygen ions. Also, the oxygen atom is located at the corners of the tetrahedra and links two tetrahedra. In the structure of the NCASO phosphor, Na^+ and Ca^{2+} ions occupy the same sites due to substitution of Na^+ for Ca^{2+} site and there is Si^{4+} or an Al^{3+} ion in the middle of each tetrahedron. Because the Al^{3+} substitutes for Si^{4+}, the charge balance is maintained by the addition of an interstitial alkali or alkaline-earth ion (Na^+ or Ca^{2+} ions).[15,16] Also, Na^+/Ca^{2+} ions have four different cases of coordination environments. Na/Ca (1), Na/Ca (2), and Na/Ca (4) are defined as being 8-

dx.doi.org/10.1021/ic300956m | Inorg. Chem. 2012, 51, 10688–10694

coordinated; Na/Ca (3) is defined as being 10-coordinated. Typically, the effective radii (r) of cations are changed depending on the coordination number (CN).[21] Therefore, the ionic radii of Eu^{2+} ions (r = 1.25 Å when CN = 8, r = 1.35 Å when CN = 10) are similar to those of Ca^{2+} ions (r = 1.12 Å when CN = 8, 1.23 Å when CN = 10) and Na^{+} ions (r = 1.18 Å when CN = 8, 1.24 Å when CN = 9, 1.39 Å when CN = 12). In the view of effective ionic radii, Eu ions are expected to occupy the Na/Ca sites preferably because both four-coordinated Al^{3+} (r = 0.39 Å) and Si^{4+} (r = 0.26 Å) sites are too small for Eu ions to replace them.

Figure 3 demonstrates the data (circled), fitted (red line), and difference (bottom) XRD profiles for the Rietveld

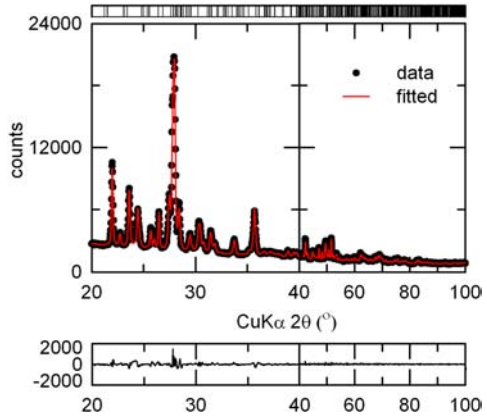

Figure 3. Rietveld refinement results of the powder X-ray diffraction profile of $Na_{0.34}Ca_{0.66}Al_{1.66}Si_{2.34}O_8$ phosphors. Expected reflection positions are displayed using vertical lines.

refinement of $Na_{0.34}(Ca_{0.93}Eu_{0.07})_{0.66}Al_{1.66}Si_{2.34}O_8$ phosphor. NCASO:Eu^{2+} crystallized in a triclinic unit cell with space group number 2 and cell parameters are a = 8.1883(3) Å, b = 12.8845(5) Å, and c = 14.2050(5) Å, and cell volume = 1345.2825 $Å^3$. The refinement finally converged to R_p = 2.48%, R_{wp} = 3.32% and χ^2 = 1.88 is demonstrated in Table 1. Also, additional refined structural parameters for $Na_{0.34}Ca_{0.66}Al_{1.66}Si_{2.34}O_8$:$Eu^{2+}$ are displayed in Table S1 of the Supporting Information.

3.2. Photoluminescence Properties of the NCASO:Eu^{2+} Phosphor. Parts a and b of Figure 4 show the Eu concentration dependence of the relative PLE/PL intensity of $Na_xCa_{1-x}Al_{2-x}Si_{2+x}O_8$:$yEu^{2+}$ (x = 0.34) phosphor, where y = 1, 3, 5, 7, 9, 11 mol %. Part a of Figure 4 indicates the PLE spectrum which shows a broad absorption band ranged at 250−420 nm. It corresponds to the $4f^7 \rightarrow 4f^65d^1$ transition of Eu^{2+} ions. The excitation intensity increases and move to longer wavelength especially in near-UV region during increasing the Eu^{2+} concentration from Eu 1 mol % to Eu 7 mol %. It is found that the NCASO:Eu^{2+} phosphor can be a promising candidate for UV-pumped white-emitting lighting. Under 365 nm excitation, the NCASO:Eu^{2+} phosphor produce very broad blue emission band peaking at around 445 nm which corresponds to the typical $4f^65d^1 \rightarrow 4f^7$ transition of Eu^{2+} ion. The emission spectrum comprises a superposition of four Gaussian bands centered at averagely 415, 440, 470, and 520 nm (orange, purple, pink, royal blue line) that were ascribed to four different emission sites on this phosphor and it can also be identified by the refinement results that four Na^{+}/Ca^{2+} shared sites are occupied by Eu^{2+} ions. The PL intensity and shape is

Table 1. Rietveld Refinement and Crystal Property Data of $Na_{0.34}Ca_{0.66}Al_{1.66}Si_{2.34}O_8$ Phosphor, the Numbers in Parentheses Are the Estimated Standard Deviations of the Last Significant Figure

formula	$Na_{0.34}$ $Ca_{0.66}Al_{1.66}Si_{2.34}O_8$
radiation type	Cu Kα
2θ range (degree)	20−100
T/K	295
symmetry	triclinic
space group #	2
a/Å	8.1883(3)
b/Å	12.8845(5)
c/Å	14.2050(5)
α/°	93.272(2)
β/°	115.870(1)
γ/°	90.549(2)
Z	8
R_p	2.48%
R_{wp}	3.32%
χ^2	1.88

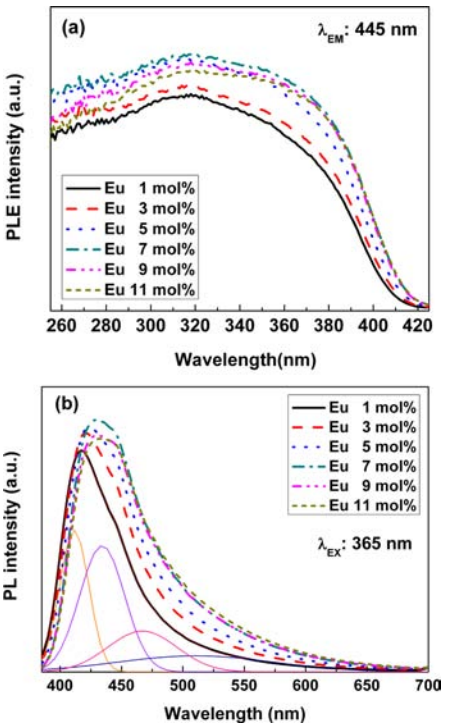

Figure 4. Excitation (a) and emission (b) PLE/PL spectra of NCASO:yEu^{2+} (y = 0.01, 0.03, 0.05, 0.07, 0.09, 0.11) phosphor with different Eu^{2+} concentrations.

also affected by Eu concentration. With increasing Eu concentration, the intensity increases and reaches a maximum value at a Eu 7 mol %. Above this value, the intensity tends to decrease due to concentration quenching effect. Also, the peak positions and shape were slightly changed and red-shifted as increasing Eu^{2+} content in the crystal structure. The reason for gradual changes of the emission band as the concentration of Eu^{2+} increases can be explained by relative intensity among the four Gaussian components (Eu1−Eu4). There are four substitutional sites of Na^{+}/Ca^{2+} ion for Eu^{2+} ion. As shown in Figure S2 of the Supporting Information, each of the deconvoluted Gaussian components indicates the transition of

dx.doi.org/10.1021/ic300956m | Inorg. Chem. 2012, 51, 10688−10694

Eu^{2+} in NCASO:Eu^{2+} phosphor. By substitution of Na^{+}/Ca^{2+} sites with Eu^{2+} ion (with increasing Eu^{2+} concentration), the relative intensity among the four Gaussian components changed as shown in Figure S2 of the Supporting Information and the central wavelength (λ_{center}) and relative intensity ($I_{relative}$) with Eu^{2+} concentration was indicated in Table S2 of the Supporting Information. These results indicate the energy transfer occurred among Eu1−Eu4 as increasing Eu^{2+} concentration. Consequently, the intensities originated from Eu2, Eu3, and Eu4 increased relatively and it affected change of emission shape.

To investigate the concentration quenching phenomena of the phosphor, critical distance (R_c) was calculated. There are two common methods for determination of critical distance (R_c). First, the critical distance (R_{c1}) between Eu^{2+} ions for energy transfer can be calculated using the relation that was proposed by Blasse and Grabmaier,[22]

$$R_{c1} \approx 2\left(\frac{3V}{4\pi X_c N}\right)^{1/3} \quad (1)$$

where V is a volume of the unit cell, X_c is the critical concentration of activator ion, and N is the number of formula unit per unit cell. In case of NCASO:Eu^{2+} phosphor, $X_c = 0.07$, $V = 1345.28$ Å^3, and $N = 8$. Therefore, R_{c1} was calculated to be 24.33 Å. In addition, the critical distance R_{c2} could be obtained from Dexter's formula. Assuming the electric dipole−dipole interaction between Eu^{2+} ions, R_{c2} can be given as

$$R_{c2}{}^6 = 0.63 \times 10^{28} \frac{4.8 \times 10^{-16} \cdot P}{E^4} \int f_s(E) f_a(E) \mathrm{d}E \quad (2)$$

where P is oscillator strength of the Eu^{2+} ion. E is the energy of maximum spectral overlap and $\int f_s(E) f_a(E) \mathrm{d}E$ is the spectral overlap integral from the normalized excitation and emission spectrum of NCASO:Eu^{2+}. P is 0.01 for an allowed 4f−5d transition, and the values E and $\int f_s(E) f_a(E) \mathrm{d}E$ were calculated to be 3.1 and 0.0261 eV^{-1} from the spectra, respectively. It turn out that R_{c2} was calculated to be 25.18 Å.

From the results, it was confirmed that the energy transfer between Eu^{2+} ions in NCASO:Eu^{2+} phosphor was mainly 4f−5d allowed electric-dipole interaction and the optimized concentration (0.07 mol) obtained.

Moreover, the concentration quenching can be explained in more detail by time-resolved measurement. Normalized decay curves for $Na_xCa_{1-x}Al_{2-x}Si_{2+x}O_8$:$yEu^{2+}$ ($x = 0.34$, $y = 1$, 3, 7, 11 mol %) phosphor under laser excitation at 375 nm are shown in Figure 5. Part a of Figure 5 shows that the decay curves were analyzed at the maximum of 0.01Eu^{2+} emission at 420 nm. The lifetime (τ) of Eu^{2+} $4f^65d^1 \rightarrow 4f^7$ emission was measured at various Eu^{2+} concentrations. The decay curve gradually got less linear as increasing Eu^{2+} concentration, which is a typical sign of energy transfer, and eventually causes concentration quenching, and this will be discussed later. The decay curve result shows that the lifetime of Eu^{2+} decreases with increasing Eu^{2+} concentration. Especially, the lifetime of Eu^{2+} decreased from 0.577 μs to 0.490 μs when Eu^{2+} concentration increased from 1 to 11 mol %. The measured lifetime is related to the total relaxation rate, which can be described by;[23,24]

$$\frac{1}{\tau} = \frac{1}{\tau_0} + A_{nr} + P_t \quad (3)$$

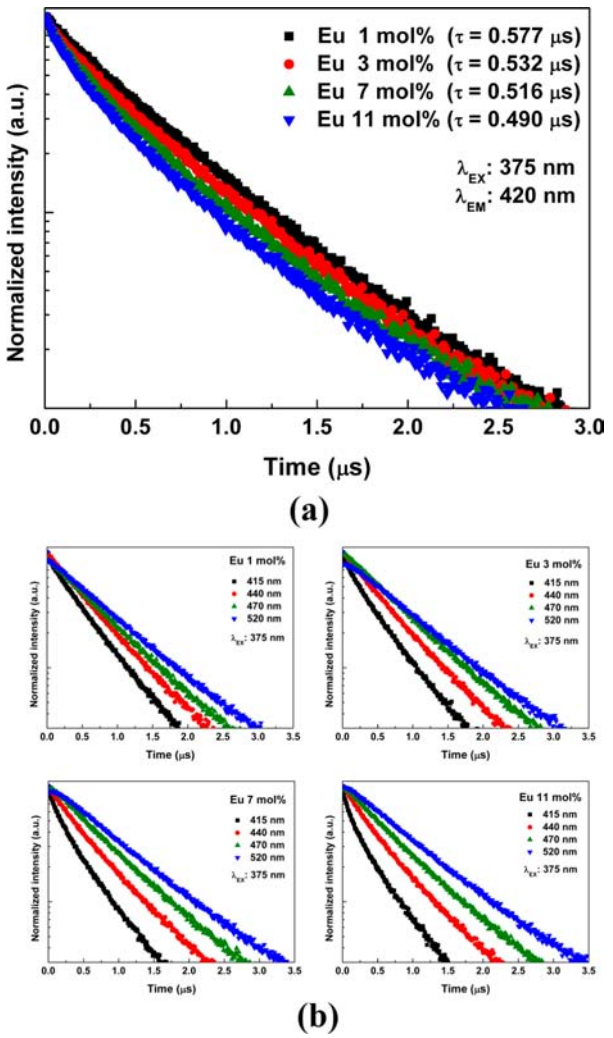

Figure 5. (a) Decay curves of Eu^{2+} emission for NCASO:yEu^{2+} (y = 0.01, 0.03, 0.07, 0.11) phosphors under excitation at 375 nm. (b) Decay curves detected at various emission wavelengths for various Eu^{2+} concentrations.

Where τ_0 is the radiative lifetime, A_{nr} is the nonradiative rate due to multiphonon relaxation, and P_t is the energy transfer rate between Eu^{2+} ions. With increasing Eu^{2+} concentrations, the distance between Eu^{2+} ions reduces. Therefore, both the energy transfer rate from Eu^{2+} to Eu^{2+} and the probability of energy transfer to killer site (such as defects) increased. As a result, the lifetimes are shortened as increasing Eu^{2+} concentration due to favoring the nonradiative energy transfer processes between Eu^{2+} ions.[25] The experimental investigation on decay times also supports that concentration quenching occurs in NCASO:Eu^{2+} phosphor.

In addition, the energy transfer can be explained more accurately using part b of Figure 5 graph, which shows decay curves detected at various emission wavelengths (related with four Eu site of NCASO:Eu^{2+} phosphor) for various Eu^{2+} concentrations. The decay curves in part b of Figure 5 also become nonlinear not only as increasing Eu^{2+} concentration but also as decreasing detecting wavelength. This result shows typical decay behavior of donors with a higher acceptor density in the vicinity.[26,27] Therefore, this nonlinearity in the donor side is more superior for the higher Eu^{2+} concentrations, which describe the brisk site to site energy transfer in higher Eu

dx.doi.org/10.1021/ic300956m | Inorg. Chem. 2012, 51, 10688−10694

concentration due to shortened interactivator distance. Moreover, the acceptor component in the lower energy side becomes more preferred when the donors in the other side were weakened as Eu concentration increased and consequently the higher energy (shorter wavelength) side is quenched. These results can be an evidence of energy transfer (concentration quenching) and red-shift phenomena.[27,28]

The appropriate emission area, luminescence intensity, and quantum efficiency of a phosphor are important facts for actual application. Figure 6 shows a comparison of the PL spectra of

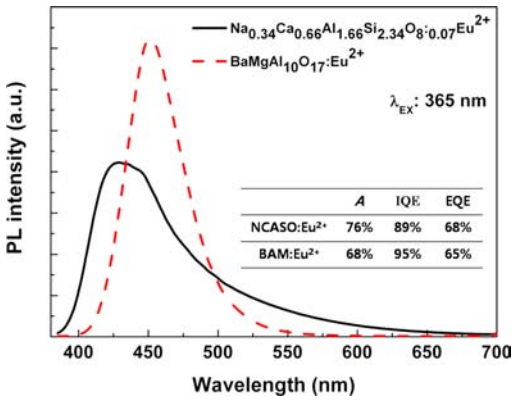

Figure 6. Comparison of PL spectra of NCASO:$_{0.07}Eu^{2+}$ with that of commercial BAM:Eu^{2+} phosphor under 365 nm excitation.

NCASO:$_{0.07}Eu^{2+}$ with that of commercial BAM:Eu^{2+} phosphor (KEMK63/F−P1, Phosphor Technology Ltd.). Under 365 nm excitation, the PL intensity area of NCASO:Eu^{2+} was measured to be 99.72% of that of BAM:Eu^{2+}. Also, NCASO:Eu^{2+} phosphor has a broader band than BAM:Eu^{2+} phosphor and its value of the full width at half-maximum (FWHM) is about 76 nm, which is due to luminescent centers located at different environments in the host material. In an industrial application field, the broader emission band is helpful for high CRI index and high efficiency when fabricating WLEDs.

To determine the absolute quantum efficiency of photo conversion for phosphor, optical absorbance (A) and quantum efficiency (Φ) of the sample were calculated by using the following equations:[29]

$$A = \frac{L_o(\lambda)\text{-}L_i(\lambda)}{L_o(\lambda)} \quad (4)$$

$$\Phi = \frac{E_i(\lambda)\text{-}(1\text{-}A)\cdot E_o(\lambda)}{L_e(\lambda)\cdot A} \quad (5)$$

where $L_o(\lambda)$ is the integrated excitation profile when a sample is diffusely illuminated by the integrated sphere's surface, and $L_i(\lambda)$ is the integrated excitation profile when a sample is directly excited by the incident beam. $E_i(\lambda)$ is the integrated luminescence of a sample upon direct excitation, $E_o(\lambda)$ the integrated luminescence of a sample excited by indirect illumination from the sphere, and $L_e(\lambda)$ is the integrated excitation profile obtained from the empty integrated sphere (without the sample present). The internal (η_i) and external (η_o) quantum efficiencies ($A \times \Phi$) were calculated to use the previously reported equations.[30] Under 365 nm excitation, the optical absorbance (A) of NCASO:Eu^{2+} and BAM:Eu^{2+} phosphor were calculated to be 76% and 68% and the internal quantum efficiency (η_i) was 89% and 95%, and external efficiency (η_o) was 68% and 65%, respectively. These results indicated that NCASO:Eu^{2+} phosphor seems like a potential candidate for UV light-emitting diode applications.

3.3. Thermal Quenching Properties of NCASO:Eu^{2+}. For the application of high performance LEDs, the thermal stability of phosphor is one of important properties. Temperature-dependent emission spectra of NCASO:Eu^{2+} phosphor under 365 nm excitation are indicated in Figure 7. The relative

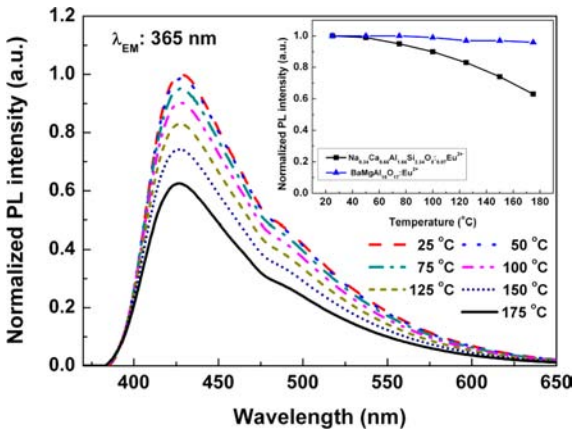

Figure 7. Temperature-dependent PL spectra of NCASO:$_{0.07}Eu^{2+}$.

PL intensity of NCASO:Eu^{2+} decreases as increasing temperature from room temperature up to 175 °C. The insert displays a comparison of thermal quenching and luminescence properties of NCASO:Eu^{2+} with that of commercial BAM:Eu^{2+} phosphor. As shown in the insert of Figure 7, we observed that the thermal stability of NCASO:Eu^{2+} could compete well with BAM:Eu^{2+} phosphor below 100 °C such that it drops only ~10%. Above 100 °C, the thermal quenching of NCASO:Eu^{2+} phosphors was much more than that of BAM phosphors.

These thermal quenching phenomena can be explained by the help of configurational coordinate diagram. With increasing temperature, electron−phonon interaction is enhanced. Through phonon interaction, the excited luminescent center is thermally activated and subsequently released through crossover between the $4f^6 5d$ excited state and $4f^7$ ground state. As a result, the emission intensity decreases due to enhanced population density of phonon.[31,32] In addition, a slight blue-shift of emission band is also observed with raising temperature. It can be explained by thermally activated phonon-assisted excitation from the excited state of the lower-energy emission band to excited state of the higher energy emission band. As increasing temperature, the electrons population in the upper vibration level of the Eu^{2+} excited state becomes dominant under phonon assistance. Thus, the radiative transition from this higher excited state makes the blue-shift behavior as temperature increases.[24,25]

To better understand the thermal quenching phenomena, the thermal quenching data were fitted using the Arrhenius equation,[33]

$$\ln\left(\frac{I_o}{I}\right) = \ln A\text{-}\frac{E_a}{k_B T} \quad (6)$$

Where I_o and $I(T)$ are the luminescence intensity of NCASO:Eu^{2+} at room temperature and a given temperature, respectively, A is constant, E_a is the activation energy for thermal quenching, and k_B is Boltzmann's constant (8.617 ×

10^{-5} eV K^{-1}). From the equation, we have obtained E_a of NCASO:Eu^{2+} to be 0.033 eV.

3.4. Electroluminescence Properties of NCASO:Eu^{2+}. WLEDs were fabricated by using near-UV LED chips (λ_{max} = 395 nm) with NCASO:Eu^{2+} phosphor, green-emitting β–SiAlON:Eu^{2+} phosphor, and red-emitting $CaAlSiN_3$:Eu^{2+} phosphor. Figure 8 shows the electroluminescent spectrum of

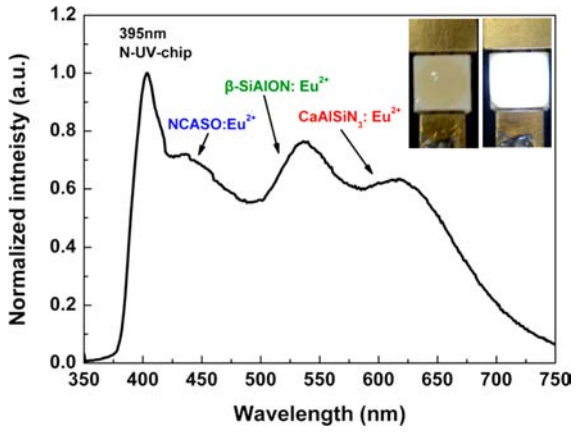

Figure 8. EL spectrum of blending three blue-emitting NCASO:Eu^{2+}, green-emitting β–SiAlON:Eu^{2+}, and red-emitting $CaAlSiN_3$:Eu^{2+} phosphor on a 395 nm emitting near-UV chip.

a fabricated WLED lamp driven under forward bias current of 20 mA. The result reveals that CIE color coordinates are (0.323, 0.335) at a warm white light correlated color temperature (CCT) of 5956 K. The full set of 9 CRIs with the color rendering index R_a = 94 is shown in Table 2. As discussed, the NCASO:Eu^{2+} can be a promising candidate for a blue-emitting phosphor for application of WLEDs.

Table 2. Full Set of 9 CRIs and the R_a of the Fabricated WLED

R_a	$R(1)$	$R(2)$	$R(3)$	$R(4)$	$R(5)$	$R(6)$	$R(7)$	$R(8)$	$R(9)$
94	98	94	89	92	96	93	92	94	88

4. CONCLUSIONS

In summary, we have reported the luminescence properties of a new blue-emitting NCASO:Eu^{2+} phosphor, which can be efficiently excited over a broad spectral range from 250 to 420 nm. The crystal structure of NCASO:Eu^{2+} was determined by the Rietveld refinement analysis. Under 365 nm excitation, we compared PL spectra and quantum efficiency of NCASO:Eu^{2+} phosphor with those of commercial BAM:Eu^{2+} phosphor, respectively. The result showed that the emission band area of NCASO:Eu^{2+} was 99.72% of that of BAM:Eu^{2+} phosphor. Also, we observed that its absorbance, internal, and external quantum efficiency are as high as 112%, 94%, and 105% of that of the commercial BAM:Eu^{2+} phosphor, respectively. The WLED fabricated with the blue-emitting NCASO:Eu^{2+}, green- and red-emitting phosphors on a near-UV LED chip demonstrated the potential of NCASO:Eu^{2+} for UV LED applications.

■ ASSOCIATED CONTENT

Ⓢ Supporting Information

Further details are given in Figure S1, S2 and Table S1, S2. This material is available free of charge via the Internet at http://pubs.acs.org.

■ AUTHOR INFORMATION

Corresponding Author

*Fax: +82-42-350-3310, tel: +82-42-350-3337, e-mail: dyj@kaist.ac.kr.

Notes

The authors declare no competing financial interest.

■ REFERENCES

(1) Nishida, T.; Ban, T.; Kobayashi, N. *Appl. Phys. Lett.* **2003**, *82*, 3817–3819.
(2) Im, W. B.; Fellows, N. N.; DenBaars, S. P.; Seshadri, R.; Kim, Y. I. *Chem. Mater.* **2009**, *21*, 2957–2966.
(3) Lee, S.; Seo, S. Y. *J. Electrochem. Soc.* **2002**, *149*, J85.
(4) Jang, H. S.; Im, W. B.; Lee, D. C.; Jeon, D. Y.; Kim, S. S. *J. Lumin.* **2007**, *126*, 371–377.
(5) Park, J. K.; Lim, M. A.; Kim, C. H.; Park, H. D.; Park, J. T.; Choi, S. Y. *Appl. Phys. Lett.* **2003**, *82*, 683.
(6) Uchida, Y.; Taguchi, T. *Opt. Eng.* **2005**, *44*, 124003.
(7) Im, W. B.; Brinkley, S.; Hu, J.; Mikhailovsky, A.; DenBaars, S. P.; Seshadri, R. *Chem. Mater.* **2010**, *22*, 2842–2849.
(8) Yang, X.; Tan, S. T.; Yu, X.; Demir, H. V.; Sun, X. W. *ACS Appl. Mater. Inter.* **2011**, *3*, 4431–4436.
(9) Wang, B.; Sun, L.; Ju, H. *Solid State Commun.* **2010**, *150*, 1460–1462.
(10) Yang, W. J.; Luo, L.; Chen, T. M.; Wang, N. S. *Chem. Mater.* **2005**, *17*, 3883–3888.
(11) Jo, D. S.; Luo, Y. Y.; Senthil, K.; Toda, K.; Kim, B. S.; Masaki, T.; Yoon, D. H. *Opt. Mater.* **2011**, *34*, 696–699.
(12) Yu, X.; Xu, X.; Yang, P.; Yang, Z.; Song, Z.; Zhou, D.; Yin, Z.; Jiao, Q.; Qiu, J. *Mater. Res. Bull.* **2012**, *47*, 117.
(13) Lü, W.; Hao, Z.; Zhang, X.; Luo, Y.; Wang, X.; Zhang, J. *Inorg. Chem.* **2011**, *50*, 7846–7851.
(14) Han, J. Y.; Im, W. B.; Kim, D.; Cheong, S. H.; Lee, G.; Jeon, D. Y. *J. Mater. Chem.* **2012**, *22*, 5374–5381.
(15) Krzmanc, M. M.; Valant, M.; Jancar, B.; Suvorov, D. *J. Am. Ceram. Soc.* **2005**, *88*, 2472–2479.
(16) Krzmanc, M. M.; Valant, M.; Suvorov, D. *J. Eur. Ceram. Soc.* **2005**, *25*, 2835–2838.
(17) Smith, J. V.; G., P. *Am. Mineral.* **1956**, *41*, 632–647.
(18) Cinnamon, C. G.; B., S. W. *Am. Mineral.* **1971**, *56*, 1180–1198.
(19) Doman, R. C. C.; C, G.; Bailey, S. W. *Am. Mineral.* **1965**, *50*, 724–740.
(20) Kroll, H.; M., W. F. *Phys. Chem. Minerals* **1980**, *5*, 255–277.
(21) Shannon, R. *Acta Crystallogr., A* **1976**, *32*, 751–767.
(22) Blasse, G. *Phys. Lett. A.* **1969**, *28*, 444–445.
(23) Imbusch, B. H. a. G. F. *Optical Spectroscopy of Inorganic Solids*; Clarendon: Oxford, 1989, p 151.
(24) Wang, D.; K., N. *J. Solid State Chem.* **2009**, *182*, 2219.
(25) Wang, D. Y.; Huang, C. H.; Wu, Y. C.; Chen, T. M. *J. Mater. Chem.* **2011**, *21*, 10818–10822.
(26) *Energy Transfer Processes in Condensed Matter*; Di Bartolo, B., Karipidou, A., Eds.; Plenum Press: New York, London, 1984, p 103.
(27) Lee, S.; Sohn, K.-S. *Opt. Lett.* **2010**, *35*, 1004–1006.
(28) Park, W. B.; Singh, S. P.; Yoon, C.; Sohn, K.-S. *J. Mater. Chem.* **2012**, *22*, 14068–14075.
(29) De Mello, J. C.; Wittmann, H. F.; Friend, R. H. *Adv. Mater.* **1997**, *9*, 230–232.
(30) Hirosaki, N.; Xie, R. J.; Kimoto, K.; Sekiguchi, T.; Yamamoto, Y.; Suehiro, T.; Mitomo, M. *Appl. Phys. Lett.* **2005**, *86*, 211905.
(31) Wu, Z.; Liu, J.; Gong, M.; Su, Q. *J. Electrochem. Soc.* **2009**, *156*, H153.

(32) Xie, R. J.; Hirosaki, N.; Kimura, N.; Sakuma, K.; Mitomo, M. *Appl. Phys. Lett.* **2007**, *90*, 191101.
(33) Huang, C. H.; Liu, W. R.; Chen, T. M. *J. Phys. Chem. C* **2010**, *114*, 18698−18701.